Journal of Power Sources 195 (2010) 214–222

Contents lists available at ScienceDirect

Journal of Power Sources

journal homepage: www.elsevier.com/locate/jpowsour

Kinetics of (reversible) internal reforming of methane in solid oxide fuel cells under stationary and APU conditions

H. Timmermann[a], W. Sawady[b], R. Reimert[b], E. Ivers-Tiffée[a,*]

[a] Institut für Werkstoffe der Elektrotechnik, Universität Karlsruhe (TH), and Karlsruhe Institute of Technology, 76131 Karlsruhe, Germany
[b] Engler-Bunte-Institut - Bereich Gas, Erdöl, Kohle, Universität Karlsruhe (TH), and Karlsruhe Institute of Technology, 76131 Karlsruhe, Germany

ARTICLE INFO

Article history:
Received 6 April 2009
Received in revised form 25 June 2009
Accepted 9 July 2009
Available online 21 July 2009

Keywords:
SOFC
Anode
Internal reforming
Ni
Methanation
Kinetics

ABSTRACT

The internal reforming of methane in a solid oxide fuel cell (SOFC) is investigated and modeled for flow conditions relevant to operation. To this end, measurements are performed on anode-supported cells (ASC), thereby varying gas composition (y_{CO} = 4–15%, y_{H_2} = 5 – 17%, y_{CO_2} = 6 – 18%, y_{H_2O} = 2 – 30%, y_{CH_4} = 0.1 – 20%) and temperature (600–850 °C). In this way, operating conditions for both stationary applications (methane-rich pre-reformate) as well as for auxiliary power unit (APU) applications (diesel-POX reformate) are represented. The reforming reaction is monitored in five different positions alongside the anodic gas channel by means of gas chromatography. It is shown that methane is converted in the flow field for methane-rich gas compositions, whereas under operation with diesel reformate the direction of the reaction is reversed for temperatures below 675 °C, i.e. (exothermic) methanation occurs along the anode. Using a reaction model, a rate equation for reforming could be derived which is also valid in the case of methanation. By introducing this equation into the reaction model the methane conversion along a catalytically active Ni-YSZ cermet SOFC anode can be simulated for the operating conditions specified above.

1. Introduction

Solid oxide fuel cell (SOFC) anodes consist of a porous, two-phase Ni-YSZ (yttria-doped zirconia) structure where electro-oxidation of the fuel takes place at the three-phase boundary fuel/Ni (electronic conductor)/YSZ (oxygen ion conductor). Nickel, homogeneously (or deliberately inhomogeneously) distributed within the anode structure, is a catalyst for a variety of reactions, the most important in the presence of steam being the reforming of methane to carbon monoxide and hydrogen according to Eq. (1):

$$CH_4 + H_2O \rightleftarrows CO + 3H_2 \quad \Delta_R H^0 = +206\,\mathrm{kJ\,mol^{-1}} \tag{1}$$

Simultaneously the water–gas shift reaction proceeds:

$$CO + H_2O \rightleftarrows CO_2 + H_2 \quad \Delta_R H^0 = -41\,\mathrm{kJ\,mol^{-1}} \tag{2}$$

For stationary or APU (auxiliary power unit) applications of SOFC systems the technologically relevant temperature range is between 700 and 1000 °C (depending on the concept and components employed) or between 600 and 800 °C (depending on the position in the stack), respectively. On the anode of an SOFC stack, reaction Eq. (1) will occur in both directions with a certain probability, as gas composition and temperature may quite significantly differ spatially. Thus, the kinetics must also consider the reverse reaction of Eq. (1) in the case of operating conditions with plenty of CO and H_2, but little CH_4 and H_2O. The reverse reaction, in turn, also not only affects the concentrations of methane, hydrogen, steam, and carbon monoxide, but also the temperature distribution since methane production generates heat. Therefore, the electrochemical performance is also affected by the reverse of reaction (1). These conditions occur in mobile APU systems during reformate operation due to partial oxidation (POX) of hydrocarbons as the CO and H_2 concentrations can vary here between 4 and 15 vol.% and 4 to 17 vol.%, respectively. The exothermic methanation reaction benefits from the fairly low mean operating temperatures (700–750 °C) which are aspired for APU systems in view of preferentially short heating-up times.

In literature, reforming and methanation on Ni have so far only been investigated separately. Studies by Bengaard et al. and Rostrup-Nielsen [1–3] for the case of reforming and by Rostrup-Nielsen et al., Takahashi et al. and Vannice [4–6] for methanation confirmed the good catalytic properties of Ni for both forward and reverse reaction. For methanation, two different mechanisms were proposed, such as the formation of carbides at the Ni surface via dissociative H_2 and CO adsorption [4] or a mechanism consisting of molecular adsorbed CO [5]. Recent results at temperatures of 600–700 °C, however, indicated that in both cases (reforming and

* Corresponding author. Tel.: +49 721 608 7490.
E-mail address: ellen.ivers@iwe.uni-karlsruhe.de (E. Ivers-Tiffée).

0378-7753/$ – see front matter © 2009 Elsevier B.V. All rights reserved.
doi:10.1016/j.jpowsour.2009.07.019

methanation) also identical mechanisms, i.e. surface carbides [1,4], can exist. According to these findings the methanation reaction can therefore, under the conditions considered by Rostrup-Nielsen et al., be described by the same (reversible) system of equations as the steam reforming of methane [4]. The investigations by Rostrup-Nielsen et al., however, also showed that the according kinetics depend on the special microstructure of the Ni catalyst chosen.

The most simple mathematical approach for reaction kinetics is in this case given by a power law according to Eq. (3):

$$r = k\, p_{CH_4}{}^{n} p_{H_2O}{}^{m} \quad (3)$$

For an investigation of the internal reforming at the catalytically active SOFC anode structures, the determination of the reforming kinetics was previously mostly carried out in powder aggregates of a Ni/YSZ mixture [7–9] and at a very low residence times.

In all cases the reaction order of methane n is between 0.85 and 1. However, Achenbach and Riensche [10] finds a reaction order of zero for steam for a Ni/YSZ cermet, whereas Ahmed and Foger and Lee et al. [11,9] obtain negative values for this parameter. In both of the latter studies, the S/C ratio was, however, always overstoichiometric with respect to the reforming reaction (S/C > 1). This goes along with a large amount of excess steam which possibly adsorbs on the anode, blocking catalytically active sites for methane reforming. This can lead to a decrease of the reforming rate with increasing steam partial pressure and would explain the negative reaction order of steam.

The activation energies E_A for methane reforming determined for the temperature range above 600 °C in the references cited above range from 50 to 135 kJ mol^{-1}. However, similar experiments under conditions in which methane can be formed via the reverse reaction of Eq. (1) in Ni/YSZ anode structures with gas flowing through the cell are not available. Methanation is treated in detail by Schulz [12] with the focus on selective CO removal after methane reforming on Ru, and Vannice [6] reviewed that this reaction takes place best on the elements Ru, Fe, Ni, Co, Rh, and Pt.

The methanation at Ni catalysts is investigated in these references especially for temperatures below 500 °C, conversion also at up to 700 °C is only treated by Rostrup-Nielsen et al. and Takahashi et al. [4,5]. The reaction orders in the case of Ni are found to range from $n_{CO} = -1{,}8$ to 1 for CO, and from $n_{H_2} = -1$ to 3 for H_2. The negative exponents are valid especially in the case of high reactant concentrations and low temperatures. In these cases the reactants occupy the surface of the Ni catalyst, thereby blocking the active reaction centers and thus inhibiting the methanation reaction. Activation energies determined for the methanation at Ni catalysts range from −69 to 160 kJ mol^{-1}, depending on whether gas diffusion in the pores limits the reaction rate, or if a surface reaction is the rate-determining step. The negative value for the activation energy was determined by Takahashi et al. for temperatures between 600 and 700 °C [5], this value being accounted for by a mechanism involving the formation of CHO species, the rate-determining step being the hydrogenation of adsorbed CHO.

The reforming at Ni/YSZ anode structures during cell operation (with and without electrical load, in combination with steam formation) was treated in several papers in recent years [10,13–16]. The housing geometries in these experiments, however, did not correspond to the stack geometries, resulting in flow conditions different from those in an SOFC stack. Since both the microstructure of a Ni/YSZ anode (porosity, tortuosity, anode thickness, Ni grain size, Ni surface area) and the conditions of the according flow field have a large influence, measurements have to be carried out under appropriate operating conditions in order to determine the valid formal kinetics. For a methane-rich operating gas under internal reforming conditions such investigations have been performed by Ahmed and Foger [11] and Timmermann et al. [17]. However, no investigations have been reported so far for Ni/YSZ anode structures that correspond e.g. to an APU operation with POX reformates, i.e. where methanation may also occur alongside the cell.

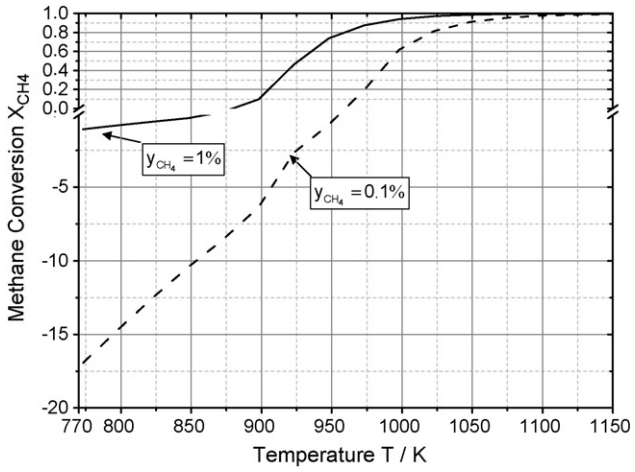

Fig. 1. Methane conversion in thermodynamic equilibrium in dependence of temperature with $y_{H_2O} = 0.06$, $y_{CO_2} = 0.1$, $y_{CO} = 0.15$, $y_{H_2} = 0.17$, balance: N_2.

Based on such measurements, formal kinetics can then be incorporated into more simple models without any complicated mechanism and without time-consuming computational procedure.

In the present paper, therefore, (i) internal reforming and (ii) methanation alongside a Ni/YSZ anode structure in a cell under operation and under appropriate stack operating conditions are investigated online. Formal kinetics for these reactions shall be determined on a purely empirical basis from measurements carried out under varying temperature, gas concentration and gas flow. A high-performance anode-supported cell (ASC) is used that consists of an anode support layer (ASL) and an anode functional layer (AFL) made of Ni/YSZ. Gas flow (500–1000 ml min^{-1}) and flow field geometry are chosen in a way that corresponds to the conditions in a planar stack. The temperature range under investigation for reforming and methanation lies between 600 and 850 °C.

2. Thermodynamics

As the reforming reaction is endothermic, the equilibrium methane conversion is expected to increase with increasing temperature. This relationship is shown in Fig. 1 in a model calculation using the process simulation software Aspen Plus® for two different methane mole fractions at the anode gas inlet (0.1% and 1% CH_4). At lower temperatures, methane conversion becomes negative, hence the equilibrium of Eq. (1) is shifted towards the educts (H_2O and CH_4) resulting in methane formation. According to Le Chatelier's principle, the less methane is present in the educt gas, the more methane is formed thermodynamically (corresponding to a negative conversion in Fig. 1). Larger mole fractions at the gas inlet therefore result in a positive-only conversion. Model calculations with different S/C ratios (S/C = 1, 2, 3), as shown in Fig. 2, indicate that higher temperatures and higher H_2O contents promote the conversion, as an increase of the H_2O educt fraction shifts the equilibrium towards the products. This trend, though, is reversed below 650 °C as methane is increasingly converted to solid carbon at lower temperatures and smaller S/C ratios. Above 850 °C, a methane conversion of nearly 100% can be achieved under the conditions investigated here up to the equilibrium, whereas in extreme cases at 600 °C already for 0.1% methane at the reactor inlet almost the 8-fold amount of methane can be formed.

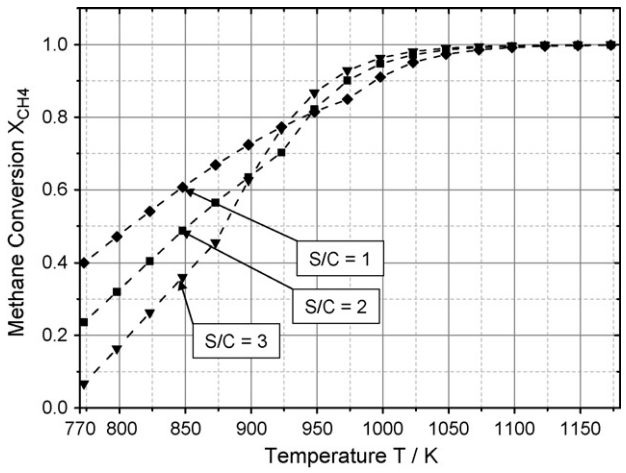

Fig. 2. Methane conversion in thermodynamic equilibrium in dependence of temperature with $y_{CH_4} = 0.1$, $y_{CO_2} = 0.1$, $y_{CO} = 0.15$, $y_{H_2} = 0.17$, balance: N_2.

3. Experimental

In our measurements at an anode-supported cell (ASC), the distribution of the anode gas composition along the gas channel was monitored by *on-line* gas analysis. Measurement setup, ASC cell characteristics and variation of temperature, gas composition, and gas flow are described in the subchapters below.

3.1. Measurement setup

The measurement setup is shown in Fig. 3. The appropriate fuel gas flow and composition is computer-controlled by digital mass flow controllers (MFC) with a control range from 5 to 3000 ml min^{-1} (under standard conditions). On the cathode side, one MFC is available for air, oxygen or nitrogen supply. On the anode side, five gases (H_2, CH_4, CO, CO_2, N_2) can be mixed according to the desired mole fractions at the gas inlet and are then led to the anode flow field. Additionally, two evaporators for liquids (water, higher hydrocarbons) are available, their volume flows can be varied over a control range of 4–600 μl min^{-1} using suitable mass flow controllers. The anode flow field (cf. Fig. 4) consists of 16 channels with a width of 1.5 mm, a height of 1.5 mm, and a length of 40 mm. The width of the bars between the channels is 1.1 mm. Alongside the anode flow field five gas samples can be extracted in situ during operation in equal distances between inlet and outlet using Al_2O_3 tubes. The gas composition is then immediately analysed with a Micro-GC (Varian CP4900). Fig. 5 shows the Al_2O_3 housing which is located in the high-temperature part of the measurement setup and into which the ASCs are inserted. Electrical contacts are applied on the cathode side by two point-welded gold meshes (net thickness 200 μm, 1024 meshes cm^{-2}). On the anode side, 2 point-welded Ni meshes (net thickness 200 μm, 900 meshes cm^{-2}, wire thickness 0.15 mm) are employed which ensure a homogeneous current distribution over the electrode. A contact weight of 1115 g ensures a reliable contacting. Sealing against air is ensured on the anode side by high-precision Al_2O_3 frames with thicknesses matching the thickness of the anode substrate.

The cells that were employed for the measurements were manufactured at the Forschungszentrum Jülich.

The anode substrate consisted of Ni/8YSZ with a support layer thickness of 1 mm and a porosity of approximately 40% (mean pore sizes around 600 nm), an anode functional layer of approximately 10 μm, a porosity of approximately 22% (mean pore sizes around 200 nm) and a substrate area of $5 \times 5\,cm^2$. On top an 8YSZ thin film electrolyte with a film thickness of 10 μm was sintered to gas tightness. The cathode (with approx. 40 μm thickness and an area of $4 \times 4\,cm^2$) consisted of mixed ionic electronic conducting (MIEC) LSCF ($La_{0.58}Sr_{0.4}Co_{0.2}Fe_{0.8}O_{3-\delta}$). The formation of insulating secondary phases (lanthanum and strontium zirconates) at the LSCF cathode/electrolyte interface was (largely) prevented by a screen-printed and sintered ceria (CGO: $Ce_{0.8}Gd_{0.2}O_{2-\delta}$) interlayer

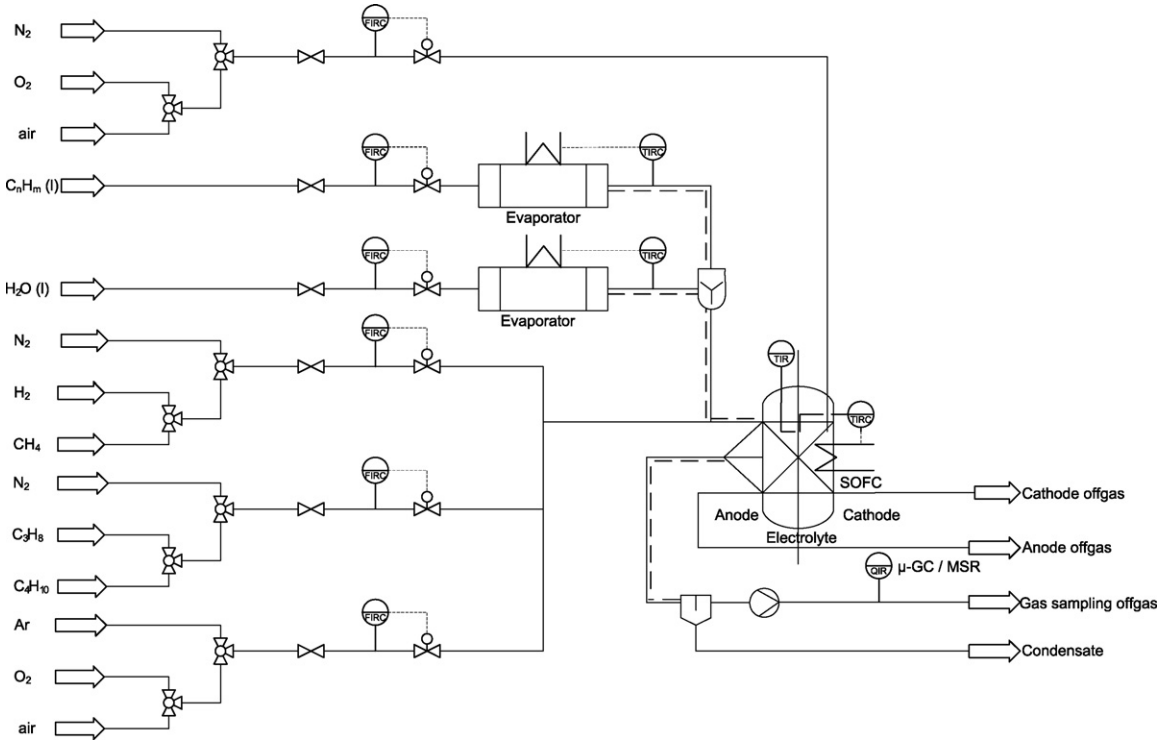

Fig. 3. Flowsheet of the measurement setup.

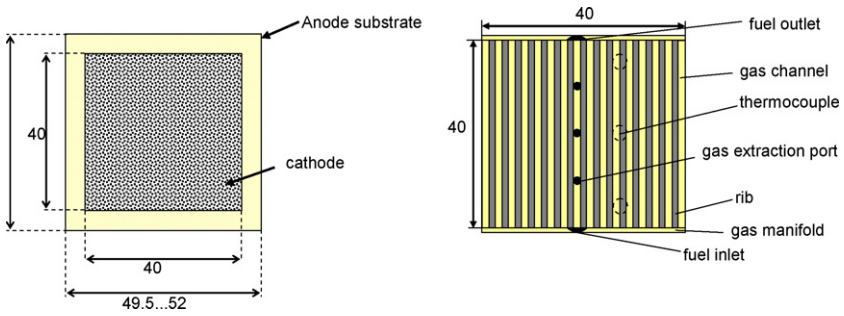

Fig. 4. View on the cathode side of the cell (left) and on the anode flow field (right).

of approximately 5 μm. Detailed information on preparation and properties of these cells is given in Refs. [18,19].

All measurements are carried out script-controlled and automated, the cell voltage is determined by a four-point measurement under constant electrical load, the corresponding cell temperature is measured by three thermocouples fitted into the anode contact block (see Fig. 4). The experimental data presented here were determined without electrical loading of the cell.

3.2. Measurements

In the experiments the mean cell temperature was varied from 600 to 850 °C and the methane mole fraction in the hydrogen fuel stepwise from 0 to 20%. Furthermore, the effect of the gas components CO, CO_2, H_2, and H_2O on the methane conversion was studied at 600 °C under conditions of operation with a synthetic reformate from catalytic Diesel partial oxidation. The fuel gas inlet flow velocity was set to a value of $v = 1\ m\ s^{-1}$, corresponding to a residence time of $\tau = 0.04$ s alongside the anode (channel length $l = 4$ cm), if not denoted otherwise. The S/C ratio (steam-to-carbon ratio), defined as the mole ratio between the amount of steam and the amount of methane, was varied from S/C = 1 to 6. The mole flow at the anode gas outlet was calculated with the help of the nitrogen mole fraction which was used as internal standard.

4. Experimental results of internal reforming

In Fig. 6, the methane conversion at the outlet of the cell ($l = 4$ cm) is shown, for $T = 750$ °C and $T = 850$ °C as a function of the S/C ratio. The methane conversion X_{CH_4} is calculated according to:

$$X_{CH_4} = \frac{{}^{N}\phi_{CH_4,in} - {}^{N}\phi_{CH_4,out}}{{}^{N}\phi_{CH_4,in}} \quad (4)$$

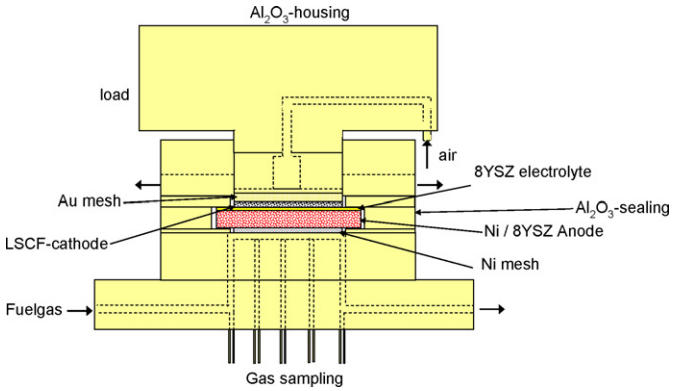

Fig. 5. Lateral view of the ceramic housing.

${}^{N}\phi_{CH_4,in}$ and ${}^{N}\phi_{CH_4,out}$ denote the mole flow of methane at the cell in- and outlet, respectively. At 850 °C, the methane conversion takes on a value of 93%, independent of the varied S/C ratio, thus not quite attaining the (theoretical) equilibrium values of 95% (for S/C = 1) and 99% (for S/C = 3). At 750 °C, a methane conversion of 80–82% is determined, which is also lower than the corresponding equilibrium values of 93% (for S/C = 1) and 98% (for S/C = 3). At 850 °C, the calculated methane conversion does not depend on the amount of methane at the cell inlet, whereas at 750 °C the methane conversion slightly decreases with increasing amount of methane in the feed, as depicted in Fig. 7.

5. Experimental analysis of methanation

For the reforming reaction (Eq. (1)), the equilibrium is shifted towards the formation of methane and steam in the cell at lower temperatures and small CH_4 and H_2O concentrations. This can be seen in Fig. 8, where the methane mole fraction at the inlet was set to values of 1% and 0.1% at 750 °C and 650 °C, respectively. At 750 °C, the methane supplied was converted along the cell; in contrast, at 650 °C and at a far lower amount of methane supplied, negative conversion is observed, implying that methane is formed within the cell. As can be seen from Fig. 9, the more CO and H_2 are present, the more methane is formed. By increasing the steam mole fraction, the equilibrium of the reforming reaction (Eq. (1)) is shifted towards the products CO and H_2, resulting in a decrease of the methane mole fraction at the gas outlet. By increasing the methane fraction at the inlet from 0.1 to 2%, the conversion approaches zero as a result of a convergence towards equilibrium composition for the operating conditions considered. However, these measurements carried out

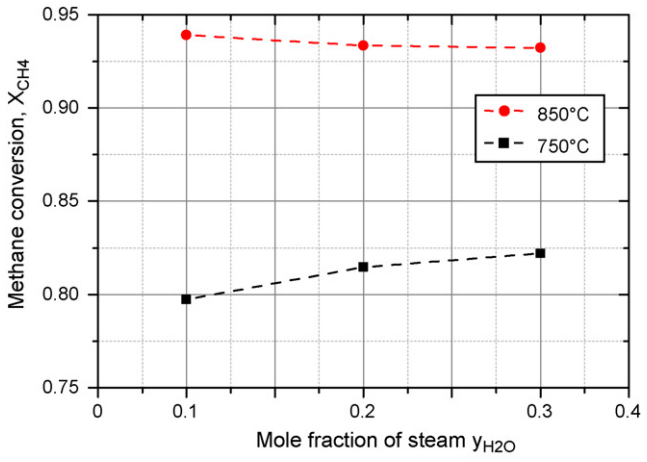

Fig. 6. Methane conversion at anode gas outlet in dependence of the S/C ratio at $y_{CH_4} = 0.1$, $y_{CO_2} = 0.1$, $y_{CO} = 0.15$, $y_{H_2} = 0.17$, balance: N_2 for two different temperatures.

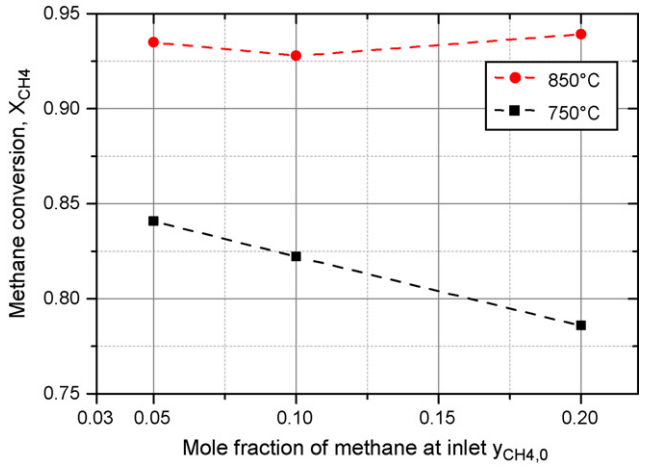

Fig. 7. Methane conversion at anode gas outlet in dependence of the methane partial pressure at $y_{H_2O} = 0.3$, $y_{CO_2} = 0.1$, $y_{CO} = 0.15$, $y_{H_2} = 0.17$, balance: N_2 for two different temperatures.

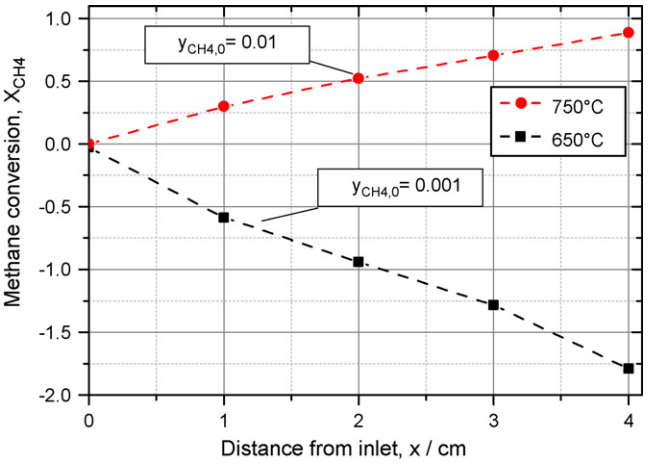

Fig. 8. Methane conversion along the anode for $y_{H_2O} = 0.06$, $y_{CO_2} = 0.1$, $y_{CO} = 0.15$, $y_{H_2} = 0.17$, balance: N_2 for two different temperatures.

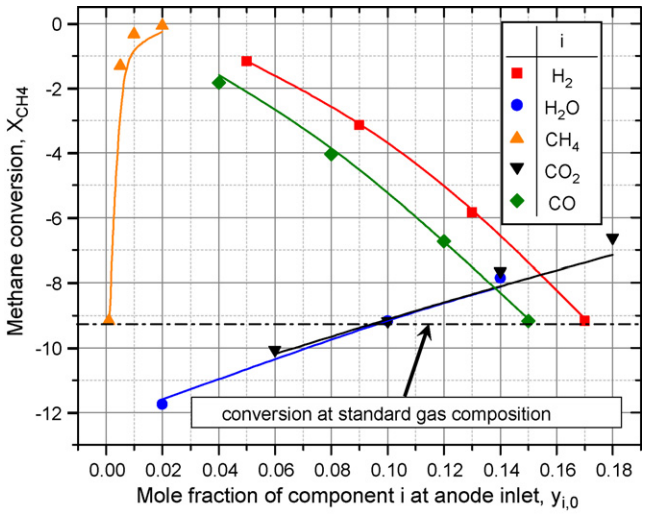

Fig. 9. Methane Conversion at anode gas outlet in dependence of the gas composition at 600 °C. Variation begins with standard gas composition $y_{CH_4} = 0.001$, $y_{H_2O} = 0.1$, $y_{CO_2} = 0.1$, $y_{CO} = 0.15$, $y_{H_2} = 0.17$, balance: N_2. Symbols account for measured values, lines for fitted values (see modeling chapter below).

with a conversion up to 93% at the cell outlet do not permit any conclusions regarding the local gas composition and the kinetics of reforming. For such statements, the development (and verification) of a reaction model is required.

6. Modeling of methane conversion

For Ni/YSZ cermets, several kinetics for the reforming reaction were determined in literature (see Table 1). It must be taken into account that composition and microstructure of the anodes investigated varied over a wide range and the operating parameters (temperature range and gas composition) at which the rate of the reforming reaction was determined also differed. The same holds for the mathematical equations and the values of the parameters employed. This leads to different expressions and to different parameter values. Therefore it is important to determine the kinetics for a technically relevant anode structure as specified above.

In the following, a mathematical model is presented for the reforming reaction on the Ni/YSZ anode described above. This model allows a quantitative assessment of the effective catalytic activity of the anode and takes into consideration both the reforming reaction (Eq. (1)) and the water–gas shift reaction (Eq. (2)). Steady state and ideal gas behavior are assumed. Diffusive gas transport in the anode gas channel over the width of the channel is neglected because the channel is very narrow (channel width 1.5 mm).

The influence of axial dispersion can be estimated by the Bodenstein number *Bo*, which is defined as the ratio of convective transport to diffusive transport [20]:

$$Bo = \frac{vl}{D_{ax}} \tag{5}$$

with the flow velocity v, the axial dispersion coefficient D_{ax} [20] and the channel length l. Axial dispersion was not taken into account in the model, because the Bodenstein number is always between 60 and 240 for methane. The temperature is considered to be constant in the cell and energy balances are not included in this version of the model. Atmospheric pressure is assumed to prevail constantly throughout the gas channel.

These assumptions reduce the number of unknown variables to 13:

- the flow velocity v in x-direction which changes because of the increase in mole flow by the steam reforming reaction (Eq. (1))
- the partial pressures of the components in the gas channel p_i, and on the external anode surface $p_{i,s}$, with $i = CH_4$, H_2O, CO, H_2, CO_2 and N_2

All these variables are a function of the coordinate x in flow direction.

With the above mentioned assumptions, the mole balance for each species can be written as:

$$0 = -\frac{d(p_i v)}{RT\,dx} - \frac{\beta_i}{d_f RT}(p_i - p_{i,s}) \tag{6}$$

with $i = CH_4, H_2O, H_2, CO, CO_2, N_2$; d_f denotes the height of the anode gas channel which is set to 1.5 mm. The mass transfer coefficient β_i [21] for the mass transfer from the channel to the anode surface is obtained by the following equation:

$$\beta_i = \frac{3.7 D_{iM}}{d_h} \tag{7}$$

where D_{iM} is the diffusion coefficient of component i in the mixture which is calculated for each position x by the approach of Fuller described by Reid et al. [22]. d_h denotes the hydraulic diameter of the anode gas channel.

Table 1
Kinetics for methane conversion on Ni/YSZ cermet anodes (literature overview) the letter ? marks properties which are not given in the cited reference.

Author	Rate of reforming reaction	n	T (°C)	E_A (kJ mol^{-1})	Anode thickness (μm)	Porosity (%)	Anode composition (wt%)
Achenbach and Riensche [10]	$r_{CH_4} = -k\ p_{CH_4}^n$	1	800–1000	82	1.4 10^3	40	22% Ni/78% ZrO_2
Lee et al. [9]	$r_{CH_4} = -k\ p_{CH_4}^n p_{H_2O}^m$	1	800–1000	98.5	Crushed cermet	38	60% Ni/40% YSZ
				74.6		55	70% Ni/30% YSZ
Ahmed and Foger [11]	$r_{CH_4} = -k\ p_{CH_4}^n p_{H_2O}^m$	0.85	854–907	95	50	?	?
Dicks et al. [8]	$r_{CH_4} = -\frac{kp_{CH_4}}{\left(1 + K_H p_{H_2}^{1/2} + K_S p_{H_2O}/p_{H_2}\right)^2}$	1	700–1000	135	Crushed cermet	40–45	55% Ni/45% YSZ

In addition, Dalton's law is applied:

$$\sum_i p_i = p \tag{8}$$

The partial pressures $p_{i,s}$ of the components on the anode surface are calculated by species balances around the anode surface for each position x:

$$\frac{\beta_i}{RT}(p_i - p_{i,s}) + \upsilon_{i,r} r_r + \upsilon_{i,s} r_s = 0 \tag{9}$$

$\upsilon_{i,r}$ and $\upsilon_{i,s}$ are the stoichiometric coefficients for component i in the reforming reaction and in the water–gas shift reaction, respectively.

r_s is the area-specific conversion rate of the shift-reaction which is calculated from the equilibrium condition (see Ref. [23] for more details)

$$K_S = \frac{p_{CO_2,s} p_{H_2,s}}{p_{CO,s} p_{H_2O,s}} \tag{10}$$

For the reforming reaction a kinetic expression of the type

$$r_r = -k\, p_{CH_4,s}^n p_{H_2O,s}^m \left(1 - \frac{p_{H_2,s}^3 p_{CO,s}}{K_{ref} p_{H_2O,s} p_{CH_4,s}}\right) \tag{11}$$

is used with

$$k = k_0 \exp\left(\frac{-E_A}{RT}\right) \tag{12}$$

r_r is the reforming rate which is related to the external anode surface, k_0 a constant and E_A the activation energy of the reforming reaction. R denotes the universal gas constant and T the temperature. K_{ref} is the equilibrium constant of the reforming reaction.

This system of equations was implemented in Matlab®, where Eq. (6) was discretized and solved by the Euler method. The values of k_0, E_A, n and m were obtained by fitting the simulated values to the measurement results shown above. Table 2 lists the values determined for the parameters. In Fig. 10 the values determined for the reaction constant k in the Arrhenius form are given. The curve shows a sharp bend above T = 750 °C, resulting in a lower value for the activation energy in the temperature range between 750 and 850 °C, as compared to its value between 600 and 750 °C. Possible reasons for the occurrence of different activation energies are discussed below.

6.1. Modeling validation

Fig. 9 shows a comparison of the results from simulations and measurements at 600 °C. At this temperature, the model is able to describe the dependency of the methane conversion on gas composition very well. The temperature dependence of the methane conversion is depicted in Fig. 11 for two different methane mole fractions at the inlet. Here, too, the measured values are in good agreement with the results of the simulation. The most significant deviation between simulation and measurement is obtained for a low conversion at 700 °C. In this case, the value of the equilibrium constant, which varies by up to 7% depending on the method of its calculation, has a significant influence on the simulation results. Moreover, the experimental error is largest for low methane values. Another cause of this deviation could be due to diffusion effects in

Table 2
Values of the parameters k_0, E_A, n and m in Eqs. (11) and (12), respectively.

Temperature T (°C)	k_0 (mol/(s m^2 bar))	E_A (kJ mol^{-1})	n	m
600–750	1483	61	1	0
750–850	38	30	1	0

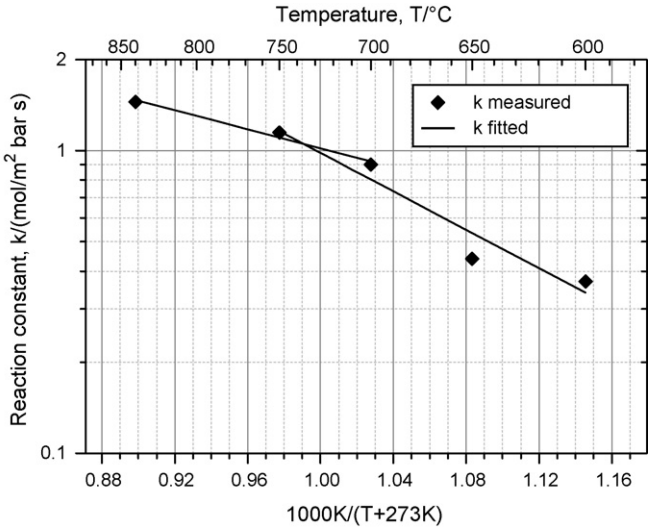

Fig. 10. Arrhenius plot of the reaction constant k_{ref} for the reforming reaction. Symbols account for measured values, lines for fitted values.

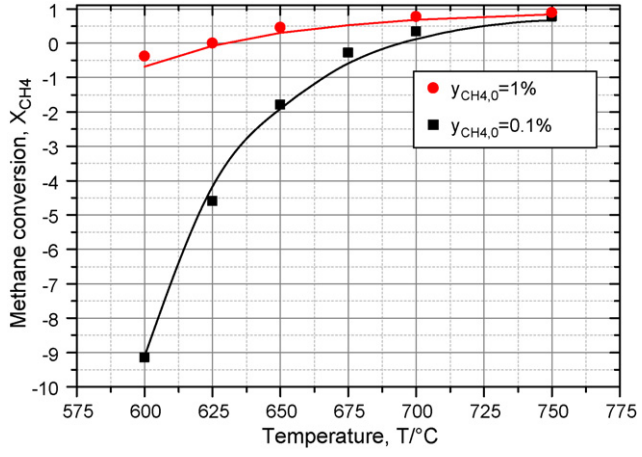

Fig. 11. CH_4-conversion as a function of temperature given for 2 methane mole fractions at anode gas inlet. Symbols account for measured values, lines for fitted values.

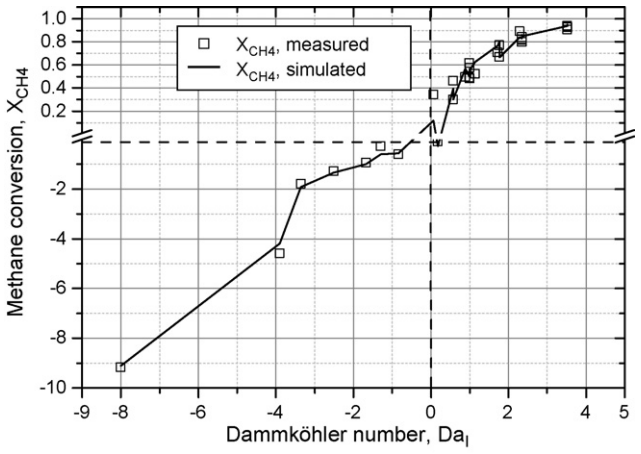

Fig. 12. CH_4-conversion as a function of the Damköhler number Da_I. Comparison of simulation results with measured values. T = 600–850 °C, $y_{H_2O} = 0.06 - 0.3$, $y_{CH_4} = 0.001 - 0.2$, $y_{CO} = 0.15$, $y_{H_2} = 0.17$, $y_{CO_2} = 0.1$, balance: N_2, v = 1 m s^{-1}, x = 1–4 cm.

the anode substrate. However, since the mean difference between simulation and measurement amounts to only 7%, the temperature dependency can be simulated over a wide range within a reasonable accuracy.

So far, only simulated results for methane conversion at the cell outlet were considered. Now, the spatial dependence and the dependence on the flow velocity are determined by using the residence time τ (according to Eq. (13)) and taking into account the local mean flow velocity $\bar{v}(x)$ (which is v averaged over x).

$$\tau = \frac{x}{\bar{v}(x)} \tag{13}$$

The simultaneous description of the methane conversion as a function of temperature and residence time succeeds by introducing the Damköhler number Da_I [24]:

$$Da_I = \frac{k_0 \exp\left(-E_A/RT\right)\left(1 - (p^3_{H_2,0} p_{CO,0}/K_{ref} p_{H_2O,0} p_{CH_4,0})\right)\tau RT}{hp} \tag{14}$$

Here $p_{i,0}$ denotes the partial pressures of the components at the reactor inlet. h is the height of the anode gas channel. As presented in Fig. 12. the simulated results fit well the measured values over a wide range of operating conditions. Negative values of the Da_I number and of conversion thereby indicate conditions, where the reforming reaction proceeds in the reverse direction, thus were methane is produced along the cell (methanation).

Since all plots that have been presented show good correlations between simulated and measured values, the model is validated for the investigated parameter range.

As a conclusion of the results presented on kinetic modeling, the kinetic expression employed seems to be appropriate to describe the rate of the methane reforming reaction and also of its reverse reaction, the methanation on a Ni/YSZ anode substrate at the operating conditions investigated. The reaction order for reforming is 1 for methane and 0 for steam, wherein steam partial pressure was varied between 0.02 bar and 0.3 bar (corresponding to a variation of the S/C ratio from 1 to 6). The presence of steam thus shows no influence on apparent kinetics over a wide S/C range, yet it influences the position of equilibrium and therefore the driving force of the chemical reaction. Hence, under methane-rich conditions, as during operation with natural gas or biogas, no influence of H_2O on the effective reaction rate and the resulting temperature balance of the stack is to be expected at an overstoichiometric S/C ratio (S/C > 1). With reformate from diesel POX, the situation is more complex: At lower temperatures first methane and H_2O are formed at the stack inlet during methanation under these conditions; then, at higher temperatures and higher fuel utilizations, which are due to the electrochemical H_2 oxidation, CH_4 is again converted in the reforming towards the stack outlet. Hence, a maximum of the CH_4 volume fraction exists in the middle section of the stack (viewed in the direction of flow), its value very strongly depends on the position of equilibrium (CO, H_2, and H_2O content and temperature) at this location. The exothermic methanation reaction that takes place in the colder inlet region leads to a heating of this part of the stack, whereas the endothermic reforming leads to a cooling at the outlet, thereby reducing the temperature gradients alongside the entire stack.

The apparent activation energies of 30 kJ mol^{-1} (see Table 2) in the range of 750–850 °C are by the factor 2–4 lower than the literature values cited in Table 1. Even in the range of 600–750 °C a value of 61 kJ mol^{-1} (see Table 2) still seems considerably low compared to the values given in Table 1**.** These considerable differences can be a result of the higher catalytic activity of the investigated anode compared to the ones described in literature. As already stated above microstructure (porosity, tortuosity, Ni active area, anode thickness) and composition of the Ni/YSZ anodes can vary. The influence of these variables becomes especially apparent in reforming catalysts where activation energies of 20–160 kJ mol^{-1} are observed [3]. Therefore, in the following the issue shall be addressed why the activation energy halves in value with increasing temperature in our measurements. Limited adsorption should lead to a reduction of the activation energy throughout the entire temperature range [20], and can hence not be the cause for its reduction by 50% for temperatures of 750 °C and above. Surface reactions come into consideration if the rate-determining step changes. With the model at hand, however, this cannot be assessed. For this purpose, an approach taking into account detailed surface reactions involving intermediates would be required as developed in Ref. [25]. One final possible cause is diffusion, potentially leading to a reduction of the apparent (formal kinetic) activation energy by approximately 50%, as compared to the intrinsic activation energy of the surface reaction [20].

The influence of pore diffusion can be estimated by the Weisz-Prater criterion with an effective pore diffusion coefficient D_{eff} and the thickness of the anode d:

$$\frac{dr_{observed}}{D_{eff} c_{i,0}} \frac{(n+1)}{2} < 0.15 \tag{15}$$

D_{eff} is calculated by the equation:

$$D_{eff} = \left(\frac{1}{\psi_j D_{i,M}} + \frac{1}{\psi_j D_{i,Kn}}\right)^{-1} \tag{16}$$

Ψ_j is the ratio of porosity and tortuosity of the anode and $D_{i,Kn}$ the Knudsen diffusion coefficient of component i:

$$D_{i,Kn} = \frac{8}{3} r \sqrt{\frac{RT}{2\pi M_i}} \tag{17}$$

where r is the mean pore radius of the anode substrate and M_i is the molar mass of compound i. For Ψ_j and r values of 0.21 and 600 μm are inserted, respectively.

If these condition in Eq. (15) is fulfilled, pore diffusion can be neglected. We obtained values between 0.1 and 1000, depending on methane inlet mole fraction and on temperature. Therefore, pore diffusion has to be taken into consideration in any case. Especially at temperatures above 750 °C the activation energy is decreased by diffusion processes in the anode substrate. Nevertheless, using the apparent activation energies of 30–61 kJ mol^{-1}, the simulation of the methane conversion on the Ni/YSZ anode is in good accordance with the measured values.

These results show that both reforming as well as its reverse reaction (methanation) can be described by a kinetic global reac-

tion rate for reaction (1) at the SOFC anode. The reforming reaction at the anode is therefore reversible under the operating conditions investigated. This behavior is in agreement with Rostrup-Nielsen's findings who determined the same activation energies for methanation on Ni as for reforming [4]. The influence of the other components (H_2, CO, and CO_2) on the methane conversion, or methanation, can be described by the reversible water–gas shift reaction and its effect on the gas composition at thermodynamic equilibrium with good precision.

Since the determined kinetics are based on an equation that allows the spatially-resolved (i.e. at each position in the direction of flow) calculation of a global reaction rate in a real anode structure, these kinetics can be introduced into the model developed in this work, which consists of 13 equations, in order to determine the concentrations along the anode with a fairly low computational effort. Hence, it can be used for system simulations facilitating the spatially-resolved calculation of (i) methane conversion, (ii) methanation, and, thus, (iii) the influence of these reactions on the gas composition within the stack. By expanding the model, the effect of these reactions on the temperature distribution can be simulated as well, as already shown in Ref. [26] in the case of reforming for a similar model.

7. Conclusions

An Ni/YSZ anode structure commonly used in planar SOFC stacks for $T \leq 850\,^{\circ}C$ was—in the form of an anode-supported cell (ASC)—subjected to several gas inlet compositions (stationary applications: methane-rich pre-reformate; APU: diesel-POX reformate). The gas conversion was monitored online under flow conditions typical of a stack by sampling at five positions alongside the flow field and subsequent ex situ analysis in a Micro-GC at temperatures between 600 and 850 °C and a volume flow of 500–1000 ml min^{-1}. Unlike previous studies, a (possible) diffusion limitation of the reactions in the anode volume is taken into account by the specific anode structure investigated (anode support layer: 1000 μm, anode functional layer: 10 μm, porosity: 30%, composition: Ni/8YSZ with an 8YSZ mass fraction of 43% before reduction of the NiO) and by the measurement setup employed in this work. It was found that

(1) at higher temperatures ($T > 675\,^{\circ}C$) and higher CH_4 concentrations ($y_{CH_4} > 1\%$), methane reforming occurs along the cell, whereas at lower temperatures ($T < 675\,^{\circ}C$) methane is formed along the cell. At the outlet (flow length 4 cm) gas compositions close to the calculated equilibrium compositions were measured in each case. For the first time, it is confirmed that the anode structure used here is not only able to catalyze the reforming reaction well, but also its reverse reaction (methanation).
(2) A pseudo-two-dimensional mathematical model was developed which describes the mass transfer resistance over the height of the flow field (channel heights 1.5 mm) in the direction of the anode surface as well as the concentration distribution in flow direction along the gas channel (channel length 40 mm).
(3) The model facilitates (by fitting the kinetic parameters to the measured data), for the first time, the determination of formal kinetics both valid for reforming and methanation. Thereby, it is shown that
    (i) the reforming reaction, including the water–gas shift reaction, is reversible in the temperature range under investigation (600–850 °C), and
    (ii) both directions of the reaction can be described by the same mechanism. This confirms the results reported by Rostrup-Nielsen et al. [4] for a Ni catalyst.
(4) For temperatures between 600 and 750 °C, the activation energies of $E_A = 60\,kJ\,mol^{-1}$ for reforming and methanation lie within the range of 50–135 kJ mol^{-1}, as reported in literature for Ni-based catalysts.
(5) For temperatures between 750 and 850 °C, the activation energies of $E_A = 30\,kJ\,mol^{-1}$ for reforming and methanation were determined. By means of an estimate using the Weisz-Prater criterion, it could be shown that in this operating range pore diffusion in the anode substrate exerts a large influence.

The formal kinetics derived in this paper are based on an equation that facilitates the spatially-resolved (i.e. at each position in the direction of flow) calculation of a global reaction rate in a technical anode substrate. Application in a model hence allows the calculation of the gas concentrations along the anode with a fairly low computational effort. Thus, these formal kinetics can be used for system simulations and enable a spatially-resolved calculation of (i) methane conversion, (ii) methanation, and, thus, (iii) the influence of these reactions on the gas composition within the stack. By expanding the model, the effect of these reactions on the temperature distribution within the stack can be simulated as well, as already shown by König et al. in the case of reforming for a similar model [26].

Acknowledgements

The authors gratefully acknowledge the collaboration of Forschungszentrum Jülich, especially with N. Menzler, who supplied the anode-supported cells. We are furthermore indebted to our colleagues A. Leonide and V. Sonn for their support in the development and design of the measurement setup. Thanks also go to S. Wagner for his support in the English translation of the manuscript.

References

[1] H.S. Bengaard, J.K. Norskov, J. Sehested, B.S. Clausen, L.P. Nielsen, A.M. Molenbroek, J.R. Rostrup-Nielsen, J. Catal. 209 (2002) 365–384.
[2] Rostrup-Nielsen, J. Steam reforming of hydrocarbons. A historical perspective. Natural Gas Conversion Vii: Proceedings of the 7th Natural Gas Conversion symposium, Dalian, China (2004) 147 121–126.
[3] J.R. Rostrup-Nielsen, Catalytic Steam Reforming, in: AndersonF J.R., M. Boudart (Eds.), Catalysis, Science And Technology, Springer, Berlin, 1983, p. P1.
[4] J.R. Rostrup-Nielsen, K. Pedersen, J. Sehested, Appl. Catal. A-Gen. 330 (2007) 134–138.
[5] N. Takahashi, Y. Shimazaki, S. Namba, T. Yashima, Zeitschrift Für Physikalische Chemie 118 (1979) 221–228.
[6] M.A. Vannice, Catal. Rev. – Sci. Eng. 14 (1976) 153–191.
[7] Drescher, I. Kinetik der Methan-Dampf-Reformierung. Dissertation, RWTH Aachen, 1999.
[8] A.L. Dicks, K.D. Pointon, A. Siddle, J. Power Sources 86 (2000) 523–530.
[9] A.L. Lee, R.F. Zabransky, W.J. Huber, Ind. Eng. Chem. Res. 29 (1990) 766–773.
[10] E. Achenbach, E. Riensche, J. Power Sources 52 (1994) 283–288.
[11] K. Ahmed, K. Foger, Catal. Today 63 (2000) 479–487.
[12] A. Schulz, Selektive Methanisierung Von Co In Anwesenheit Von Co2 Zur Reinigung Von Wasserstoff Unter Den Bedingungen Einer Pem-Brennstoffzelle. Dissertation Universität Karlsruhe, 2005.
[13] R. Kikuchi, K. Eguchi, J. Japan Petroleum Institute 47 (2004) 225–238.
[14] M.B. Pomfret, O. Demircan, A.M. Sukeshini, R.A. Walker, Environ. Sci. Technol. 40 (2006) 5574–5579.
[15] N. Nakagawa, H. Sagara, K. Kato, J. Power Sources 92 (2001) 88–94.
[16] J. Meusinger, E. Riensche, U. Stimming, J. Power Sources 71 (1998) 315–320.
[17] H. Timmermann, D. Fouquet, A. Weber, E. Ivers-Tiffée, U. Hennings, R. Reimert, Fuel Cells 6 (2006) 307–313.
[18] Buchkremer, H.P., Diekmann, U., Stöver, D. Components Manufacturing and Stack Integration of an Anode Supported Planar SOFC System. In: Thorstensen, B., (Ed.), Proceedings of 2nd European Solid Oxide Fuel Cell Forum. Oslo, Norway. 6–10 May 1996, pp 221–228.
[19] A. Mai, V.A.C. Haanappel, F. Tietz, I.C. Vinke, D. Stöver, Microstructural and electrochemical characterisation of LSCF-based cathodes for anode-supported solid oxide fuel cells, in: S.C. Singhal, M. Dokiya (Eds.), Proceedings Of The Eigth International Symposium On Solid Oxide Fuel Cells (SOFC-Viii), 2003, pp. 525–532.
[20] O. Levenspiel, Chemical Reaction Engineering, John Wiley & Sons, Hoboken, 1999.

[21] H.D. Baehr, K. Stephan, Wärme- Und Stoffübertragung, 5 Ed., Springer, Berlin, 2006.
[22] R.C. Reid, J.M. Prausnitz, B.E. Poling, The Properties of Gases and Liquids, 4 Ed., Mcgraw-Hill, New York, 1987.
[23] H. Timmermann, D. Fouquet, U. Hennings, E. Ivers-Tiffée, R. Reimert, Modelling of the methan conversion on a Ni/Cgo-anode, in: S.C. Singhal, J. Mizusaki (Eds.), Proceedings Of The Ninth International Symposium On Solid Oxide Fuel Cells (SOFC Ix), 2005, pp. 796–805.
[24] M. Baerns, H. Hoffmann, A. Renken, Chemische Reaktionstechnik, vol 1, 2 Ed., Thieme, Stuttgart, 1992.
[25] E.S. Hecht, G.K. Gupta, H.Y. Zhu, A.M. Dean, R.J. Kee, L. Maier, O. Deutschmann, Appl. Catal. A-Gen. 295 (2005).
[26] P. König, H. Timmermann, E. Ivers-Tiffée, Development and validation of a modelling tool for SOFC systems, in: J.A. Kilner, U. Bossel (Eds.), Proceedings Of The 7th European Solid Oxide Fuel Cell Forum, 2006, pp. P0903–P0945.